© Universiti Tun Hussein Onn Malaysia Publisher's Office

JSMPM

http://publisher.uthm.edu.my/ojs/index.php/jsmpm

e-ISSN : 2821-2843

Journal of Sustainable Materials Processing and Management

Synthesis and Characterization of Graphene-Cu Composite Via Hydrothermal Method

F. O. Omoniyi[1,2,3*], A. B. Alabi[2], M. A. Salawu[2], A. D. A. Buba[3]

[1]Department of Physics with Electronics, Faculty of Basic Sciences,
Ave Maria University, Piyanko, Nasarawa State, 961104, NIGERIA

[2]Department of Physics, Faculty of Physical Science,
University of Ilorin, Ilorin, 240003, NIGERIA

[3]Department of Physics, Faculty of Science,
University of Abuja, Abuja, 900211, NIGERIA

*Corresponding Author

DOI: https://doi.org/10.30880/jsmpm.2022.02.02.005
Received 18 May 2022; Accepted 03 August 2022; Available online 31 October 2022

Abstract: In recent times, composites of graphene are being produced for purposes such as electrodes and gas sensors among others. The synthesis of graphene composites was done via various methods available. Loading copper on graphene like every other transition metal to obtain composite with wide band gap has not been harnessed as such for the similar purposes. In this research, graphene-copper (G-Cu) composites were synthesized via hydrothermal method, using glucose as catalyst, with 5, 15 and 25 wt% copper compositions. In this paper, G-Cu composite is synthesized with different wt% ratio and were characterized using scanning electron microscope (SEM), X-ray diffractometer (XRD) and ultraviolet–visible spectroscopy (UV-Vis). Elastic/plastic alloy was formed by carbon and copper around $2\theta = 44°$. The grain sizes were observed to decrease proportionally with increasing temperature. The effect of composition fluctuates the XRD intensity peaks. The band gaps for 5 wt% (as-grown) reduced as temperature increases. Short calcination duration of the composites is observed to have reduced band gaps value to that of longer duration. The thermal treatment of (G-Cu) is observed to cause thermal exfoliation and elastic/plastic alloy formation by Cu and amorphous carbon.

Keywords: Graphene, calcined, wavelength, composition, optical, band-gap

1. Introduction

Graphene is a nanomaterial with wider focus, wonderful interest and attraction from researchers in nanotechnology. It is a 2-dimensional carbon allotrope and a versatile material without band gap discovered in 2004 [1]. It is the basic structural element of some carbon allotropes, including graphite, CNTs and fullerenes [2]. The atoms in graphene sheets are considered surface atoms due to their large surface area per unit volume which makes them suitable for adsorption of gas molecules [3]. Fig. 1 shows the schematic structure of graphene sheet.

Inorganic nanoparticles, such as metals or semiconductors have been introduced into the interlayer of the graphene nano sheets, in order to obtain the graphene with high individual dispersion [5,6]. The inertness of graphene, band gap and its inability to disperse in solvent [7] is observed to be a setback as it weakens the effectiveness in the synthesis of composites, semiconductors and sensors [8,9].

*Corresponding author: omoniyifrancis@gmail.com

The energy band gap of nanofilms increases with decrease in size and the trend of increasing the energy band gap with decreasing size are same as that of spherical nanosolids and nanowires [10]. He reported the following model for the energy band gap which is reasonably consistent with the available experimental data [10].

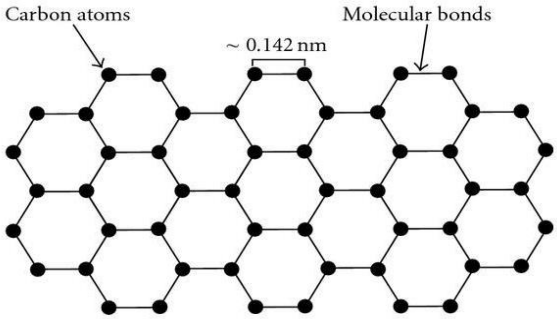

Fig. 1 - Schematic structure of a graphene sheet [4]

For spherical nanosolids, *d* is the diameter of an atom, and *D* is the diameter of the spherical nanosolids;

$$E_g(D) = E_g(bulk)(1 + \frac{2d}{D}) \quad (1)$$

For nanowire;

$$E_g(l) = E_g(bulk)(1 + \frac{4d}{3l}) \quad (2)$$

For nanofilms;

$$E_g(h) = E_g(bulk)(1 + \frac{2d}{3h}) \quad (3)$$

Where *l* is the diameter of nanowire, and *h* is the width of the nanofilm.

Graphene-based materials have shown outstanding potentials for a variety of applications, including energy storage, [11-13], bio applications [14], flexible electronics [15], sensors etc., as a result of remarkable electrical, optical, thermal, and mechanical properties [16]. These properties make graphene composites sustainable materials.

In-situ crystallization (in situ binding) and ex-situ hybridization (post-immobilization) are the two methods of loading metal nanoparticles on graphene [17]. A disadvantage of ex-situ method is the formation of non-uniform nano-structures in the composite because of lack of uniform coverage, due to non-uniformity of graphene sheets [18,19].

Many methods have surfaced recently among which the electrochemical method by Ni'maturrohmah *et al.* [20] to upscale graphene at low cost is one of them. Nevertheless, hydrothermal and solvothermal solution methods are still convenient and popular for preparing graphene-metal and graphene-metal oxide nano-composites as a result of homogeneity of constituents. For hydrothermal method, water is used as precursor while alcohol is used in solvothermal method [18].

In this paper, G-Cu is synthesized and the SEM, XRD and UV-Vis properties of the composite were studied.

2. Methodology

2.1 Reagents

Graphene oxide was obtained from Adnano technologies in India, 99.9% pure Kermel copper nitrate from China and pure glucose from Surechem Products Limited, Needham market, Suffolk in England.

2.2 Sample Synthesis

The synthesis was done using 5, 15 and 25 wt% of copper respectively. The mass ratio of each percentage composition of the mixture was done by weighing dispersible Graphene-Oxide (GO) and Copper nitrate ($Cu(NO_3)_2$). The measured samples were poured into a beaker containing 25 ml distilled water at room temperature, and the catalyst (99% pure glucose) added. Thereafter, boiling was done at 100 ˚C for 90 minutes in a pressure cooker as an alternative to

autoclave. 0.3 g of glucose was used for every 3 g of GO/$Cu(NO_3)_2$ mixture. The product was washed with distilled water twice to remove any possible acidic or alkaline content using filter paper for the filtering.

2.3 Annealing

The filtrates were left at room temperature for 24 hours. Calcination (annealing) in an oven was done at 200˚C and 400˚C for 5%, 15% and 25% respectively for 12 hours.

2.4 Structural Characterization

The structural and morphology characterization of the G-Cu samples were done using Empyrean X-ray diffractometer and scanning electron microscope (SEM) that focused beam of high electrons to evaluate the structure and morphology at 15 kV. The X-ray diffractometer used accelerating voltage of 45 kV and angle 2θ with minimum step size 0.0001° in the analyses for the synthesized G-Cu.

2.5 Optical Studies (UV-Vis Spectroscopy)

UV-Vis spectrophotometer was used to obtain the absorption spectrum of the composite within the wavelength range of 200 to 1100 nm. Prepared 0.1 M concentration of G-Cu was used for the UV-Vis spectroscopy of the 5, 15 and 25 wt% of copper using ethanol as solvent.

3. Results and Discussion

3.1 Characterization of 0.1 M Solution of G-Cu

Table 1 shows the technical details of the obtained graphene oxide (GO). The properties of the GO obtained from Ad-Nano Company, has purity level above 99% and it is dispersible. It has a very small number of layers between 1and 3, and thickness between 1 nm and 2 nm. It was produced using Hummer's method and it is an insulator that is convertible to conductor. Fig. 2 shows the diffraction peak of GO at 11.6° (JCPDS No. 75-2078). This can be rationalized to be due to the presence of oxygenated functional groups on the carbon sheets of GO. XRD in Fig. 2 also shows small peak around 21° with wider base with very low intensity, and this shows that the graphene oxide is not fully interconnected with oxygen atoms. Diffraction peak at 26.5° for little constituent of graphene while the peak at 42.5° with (100/101) planes of amorphous carbon are indications of mixture of crystalline and amorphous. On the other hand, The GO nanosheets in Fig. 3 are in flake-like shapes with the description in Table 1. It is evident from the magnification 60,000x that the sizes are very small.

Table 1 - Technical details of graphene oxide (GO)

Graphene Oxide	Description
Purity	>99%
Number of layers	1-3 layers
Average thickness (z)	1-2 nm
Average lateral dimension (x & y)	5-10 nm
Surface area	200 m^2/g
Electrical conductivity	Insulator {convertible to conductor]
Carbon %	77%
Oxygen %	22%
Others %	1%

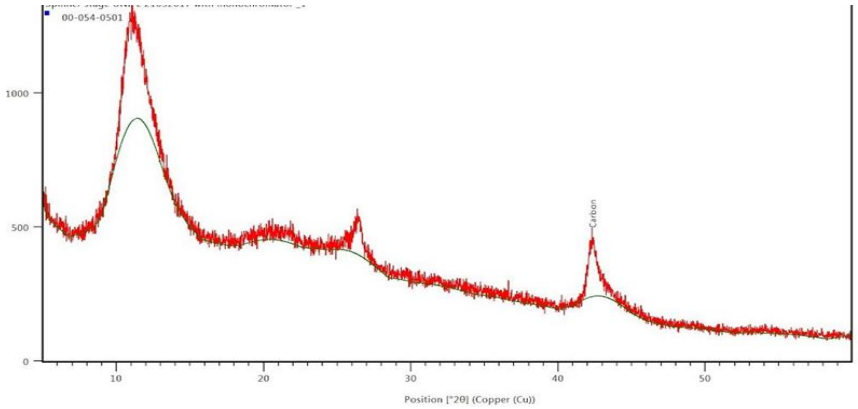

Fig. 2 - XRD pattern of GO

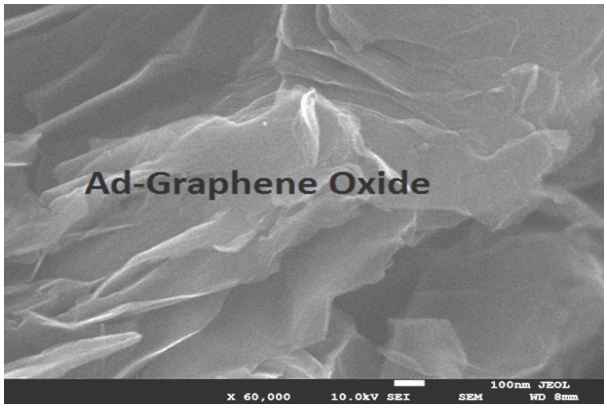

Fig. 3 - SEM micrograph of GO

3.2 Surface Morphology of G-Cu

The SEM image in Fig. 4(a) shows aggregated and stacked layers of graphene with 5 wt% loaded copper. The shapes are rutile as revealed by the 1000x magnification. This is considered to be due to stacking of graphene to become multi-wall carbon nanotubes (MWCNTs). The aggregates size in Fig. 4(b) reveals the exfoliated size of the grains at calcination temperature of 200°C, with decomposed stacked graphene at 3000x magnification, which is due to the pressure and stress created in the planes by temperature. In Fig. 4(c), the exfoliation at 400°C for 5 wt% with further grain refinement [21] is shown by the micrograph to be in flake-like form as exfoliated. The synthesized samples of 25 wt% of copper in Fig. 5(a) and Fig. 5(b) depict grains sizes reduction due to thermal exfoliation as shown by SEM micrograph and this reduced size, translates into large surface area. Fig. 5(b) is in the form of strain of spherical grains.

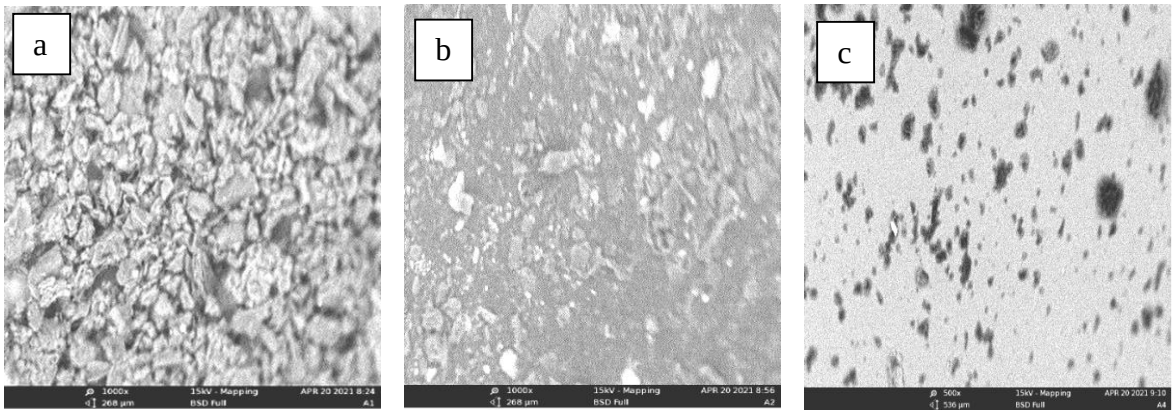

Fig. 4 - SEM micrograph of G-Cu; (a) 5 wt% copper (as-grown); (b) 5 wt% copper annealed at 200°C; (c) 5 wt% copper annealed at 400°C

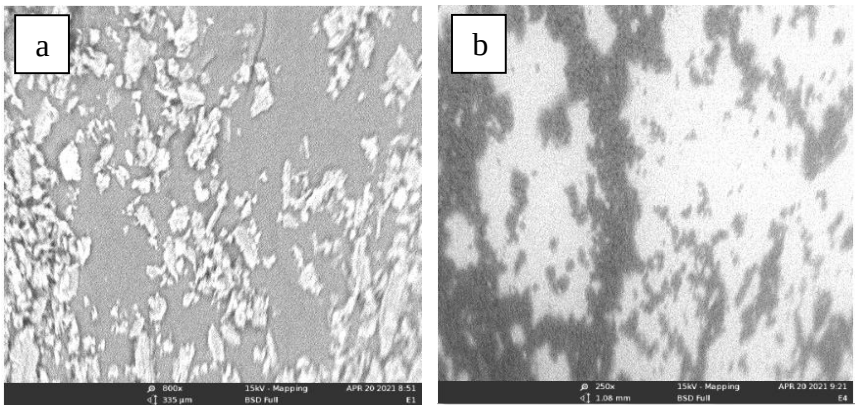

Fig. 5 - SEM micrograph of G-Cu; (a) 25 wt% copper (as-grown); (b) 25 wt% copper annealed at 400°C

3.3 Structural Analysis with X-Ray Diffraction

The peak intensity of multi wall graphene is centered at 26.5° in Fig. 6(a) (as-grown) is noticed to reduce with temperature rise when compared with Fig. 6(b) (at 400°C). This can also be attributed to decline in crystallinity and size reduction due to decomposition. This centered peak 2θ = 26.5° is associated with MWCNTs, which could be observed in a hexagonal graphite along with the diffraction line 2θ of 44° (100 plane) (JCPDS No 01-0646) [22,23]. The broad peak at 44° is that of copper-carbon alloying to form elastic or plastic alloy. At 2θ = 54.5° in both Fig. 6(a) and Fig. 6(b), the presence of graphite is observed. The average crystalline size (ACS) for Fig. 6(a) is at 26.5° and it is calculated to be 6.17 nm while at peak 44°, the ACS is 2.98 nm. The average crystalline size (ACS) for Fig. 6(b) at 26.5° is calculated to be around 3.41 nm while at 44°, the ACS is 2.80 nm.

The expected result for the composite is achieved with graphene peak at 26.5° and peaks alloying of carbon and copper at 44°. The successful incorporation of SnO_2 by Mohan *et al.* [24] into graphene using hydrothermal method experienced slight shift in the (002) peak of graphene domain and it was observed to overlap with the diffraction peak of SnO_2. Similarly, overlapping of carbon plane and copper is seen at 44° for all the X-ray diffractogram of G-Cu composite. This is attributed to the slight shift in the peaks of both carbon and copper to 44°. Similar to the simulated peaks recorded by Ni'maturrohmah *et al.* [20] that are 26.7º; 31.9º and 45.8º, for graphene loaded on copper, we recorded similar peaks for copper loaded on graphene at 26.5°, 44° and 54.5°. Licht *et al.* [25], produced electrodes for lithium-ion battery and recorded peaks as the same with that obtained in this work.

The ACS of Fig. 6(c) at 26.5° is around 4.63 nm and 3.58 nm for copper-carbon at 44°. MWCNTs is similar to an atom of graphite which is a conductor and its presence is observed at 54.5° and its intensity in Fig. 6(a) is stronger than that in Fig. 6(b). For 400°C, at 26.5° (ACS is 3.0 nm) and 44° (3.21 nm). The intensity of MWCNTs is highly reduced in Fig. 6(d) due to exfoliation of structure by thermal energy. The wide base at various peaks is an indication of amorphous constituent and it is wider in Fig. 6(d) than Fig. 6(c). Sharp and high intensity peak at 26.5° of Fig. 6(c) shows that crystalline presence is more than that of Fig. 6(d). The XRD plots have shown that glucose is able to catalyzed the removal of oxygen completely from GO.

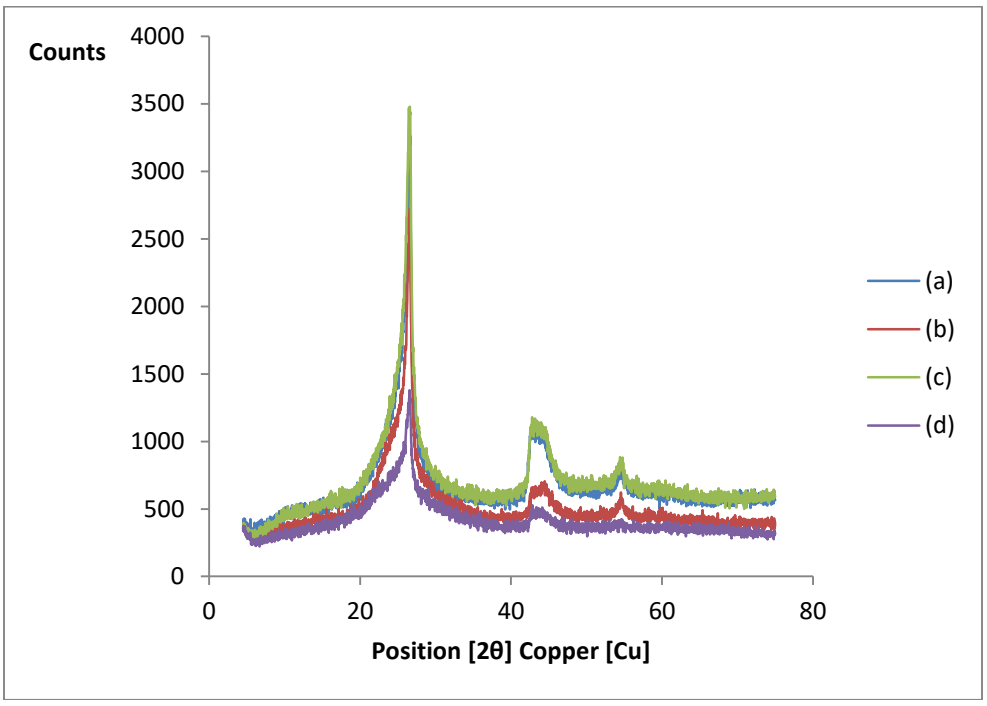

Fig. 6 - XRD; (a) 5 wt% copper in G-Cu (as-grown); (b) 5 wt% copper in G-Cu annealed at 400°C; (c) 25 wt% copper in G-Cu as-grown; (d) 25 wt% copper in G-Cu annealed at 400°C

3.4 Optical Studies (UV) of G-Cu

Fig. 7 displays the UV-Vis Spectra of the different compositions of G-Cu composites. The peak wavelength of Fig. 7(a) is at 285 nm wavelengths and absorbance intensity of 3.94 a.u. Fig. 7(b) shows the corresponding band gap of Fig. 7(a) to be 4.16 eV for 5 wt% of copper. Fig. 7(c) has peak at 285 nm with 3.02 a.u. intensity while Fig. 7(d) is the optical band gap with 4.13 eV. The peak of Fig. 7(e) is 285 nm with 3.46 a.u. and optical band gap 4.10 eV as shown in Fig. 7(f).

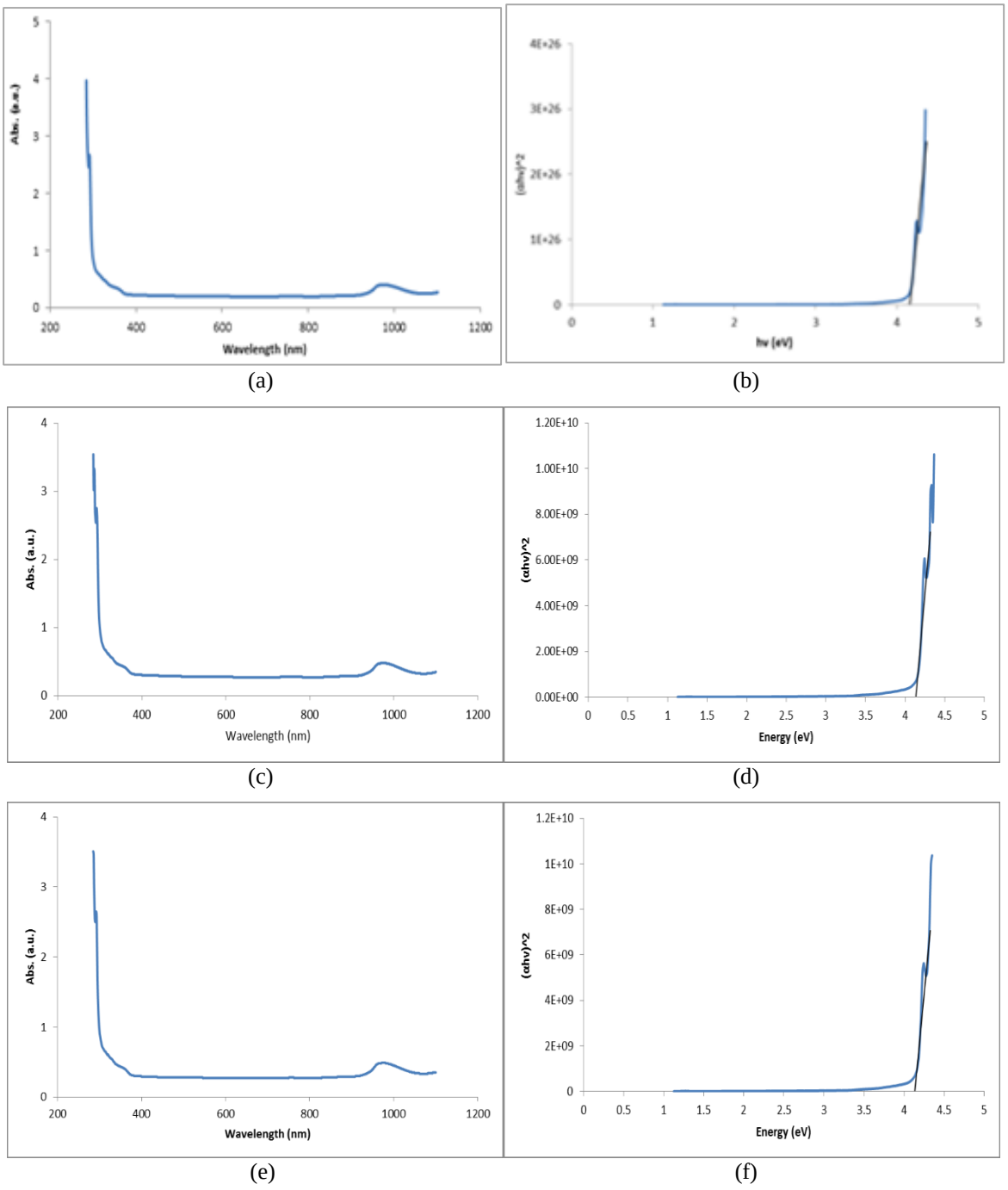

Fig. 7 - (a) Absorbance spectral of 5% Copper composition (as-grown); (b) optical band gap of 5% copper composition; (c) absorbance spectral of 15% copper composition (as-grown); (d) optical band gap of 15% copper composition; (e) absorbance spectral of 25% copper composition (as-grown); (f) optical band gap 25% copper composition

The band gap narrows with increasing copper concentration for as-grown as a result of overlapping of the dopant atoms from many body interactions. The absorbance intensity is observed to decrease with decrease in wt% of graphene in the composite. The peak at Fig. 8(a) is at 291 nm and intensity 4.2 a.u. while Fig. 8(b) shows the band gap to be 4.15 eV. In Fig. 8(c), the peak is at 292 nm with intensity 3.47 a.u. At 200°C the optical band gap is observed to reduce for 15% but rose again for 25% copper. This depicts obstruct created in the planes of the composite as a result of more elastic/plastic formation by copper-carbon.

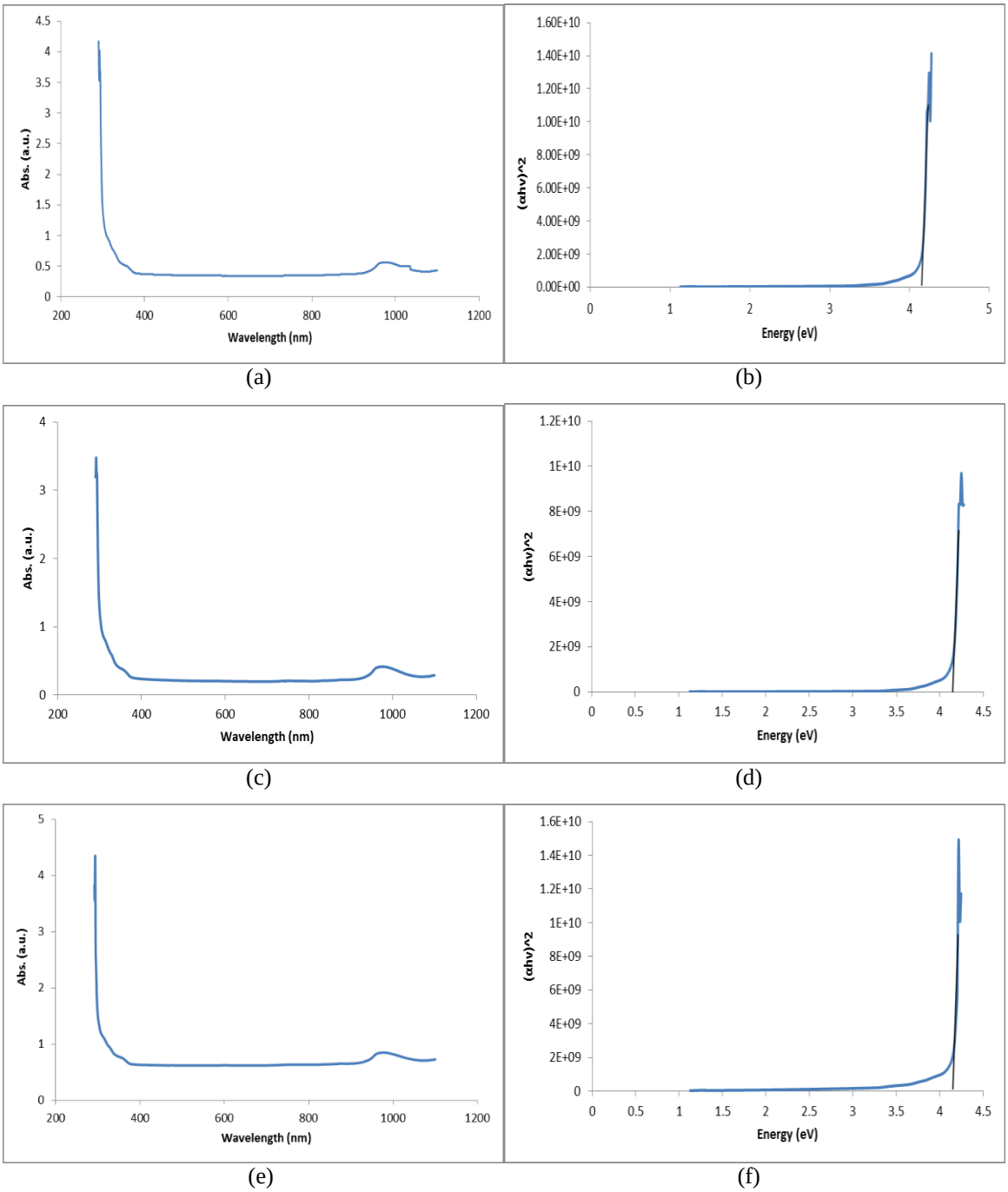

Fig. 8 - (a) 5% Copper composition of graphene-copper, annealed at 200°C; (b) optical energy band gap is 4.15 eV for 5% copper composition annealed at 200°C; (c) 15% copper composition annealed at 200°c; (d) optical band gap of 15% copper composition annealed at 200°c is 4.13 eV; (e) 25% copper composition annealed at 200°C; (f) optical band gap of 25% copper composition annealed at 200°C is 4.10 eV

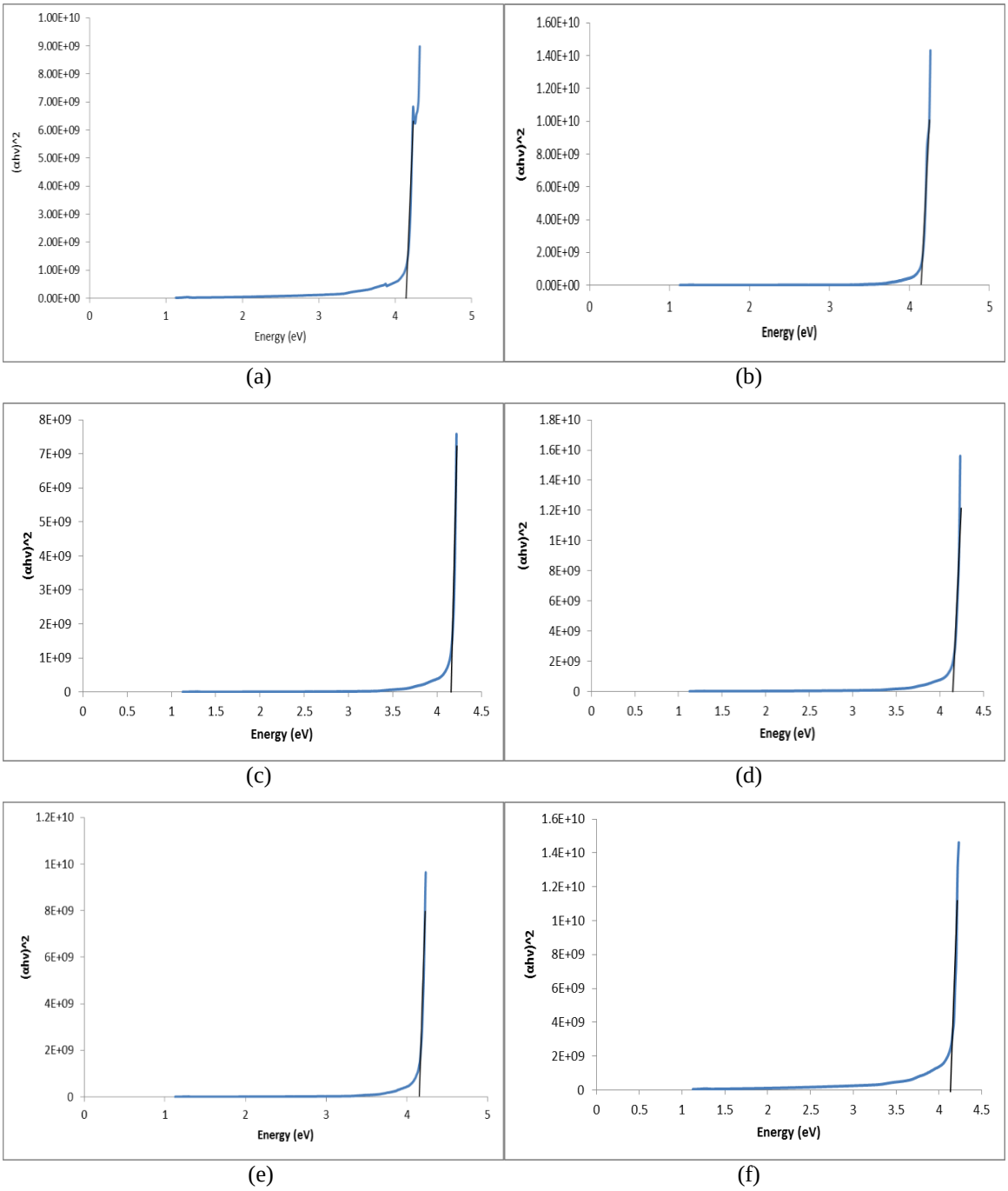

Fig. 9 - (a) Optical energy band gap of 5% copper composition annealed at 400°C for 12 hours is 4.11 eV; (b) optical band gap of 5% copper composition at 400°C annealed for 6 hours is 4.07 eV; (c) optical band gap of 15% copper composition is 4.16 eV annealed at 400°C for 12 hours; (d) optical band gap of 15% copper composition is 4.15 eV annealed at 400°C for 6 hours; (e) optical band gap of 25% of copper composition annealed at 400°C for 12 hours is 4.15 eV; (f) optical band gap of 25% copper composition annealed at 400°C for 6 hours is 4.12 eV

On the hand, Fig. 10 shows the UV-Vis spectra of 5, 15 and 25 wt% of G-Cu (as-grown). The effect of composition fluctuates the peaks as the signature peak shift between 285 nm wavelengths for 5% copper, both 15% and 25% copper compositions had peaks at 286 nm. The effect of copper concentration affects the peak due to atomic rearrangement in alignment. Fig. 11 shows the UV-Vis spectra of these compositions annealed at 200°C. At 200°C, the peak wavelength increased linearly with composition (5% with 291 nm; 15% with 292 nm; 25% with 294 nm). The dopant concentration effect on absorbance intensity observed for as-grown is noticed also at this temperature to behave as that of Fig. 10. UV-Vis spectra of G-Cu at 400°C, is shown in Fig. 12. For 400°C (12 hours), the peak wavelength is in the order 288 nm for

5 wt%, 294 nm for 15 wt% and 25 wt% copper respectively. The absorbance peak increased with temperature rise for the compositions. Higher temperature effect raised the absorbance intensity of 5 wt% above others.

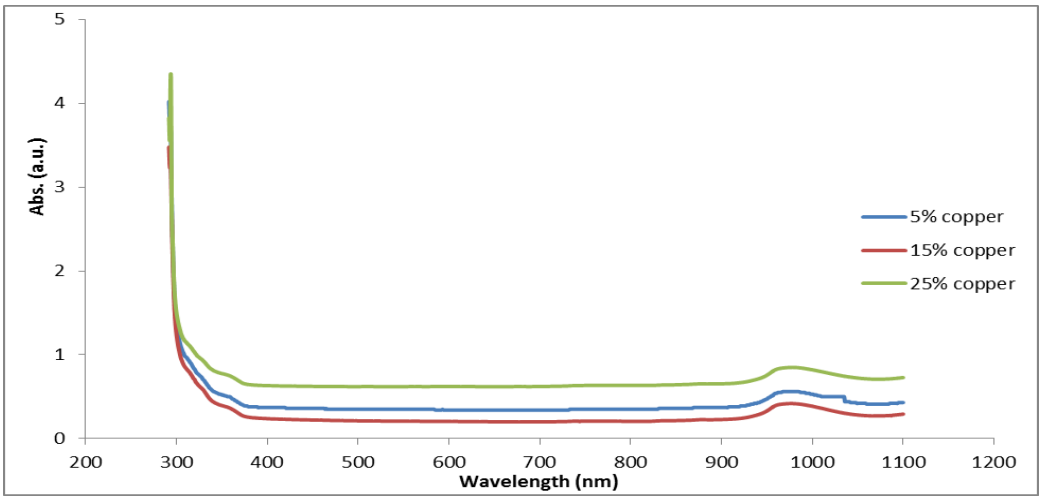

Fig. 10 - UV-Vis Spectra for as-grown

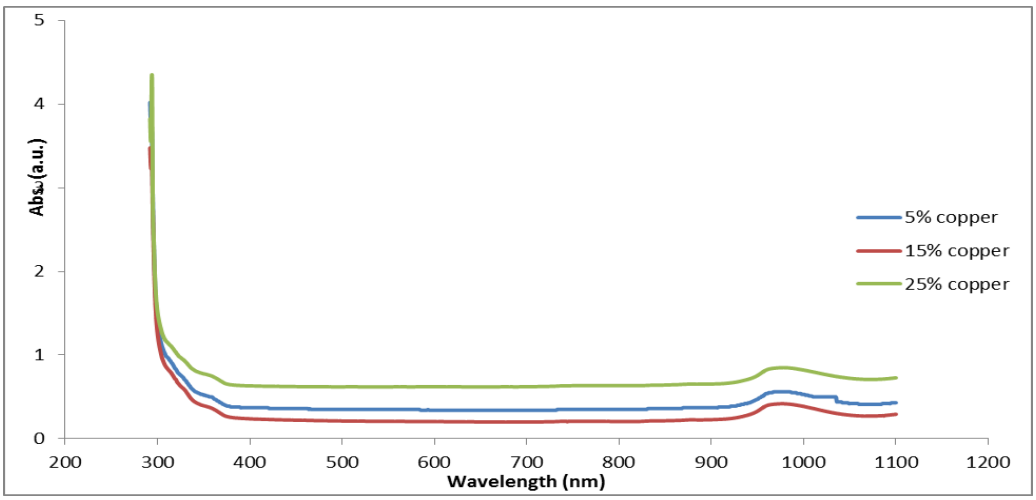

Fig. 11 - 5%, 15% and 25% copper composition annealed at 200°C

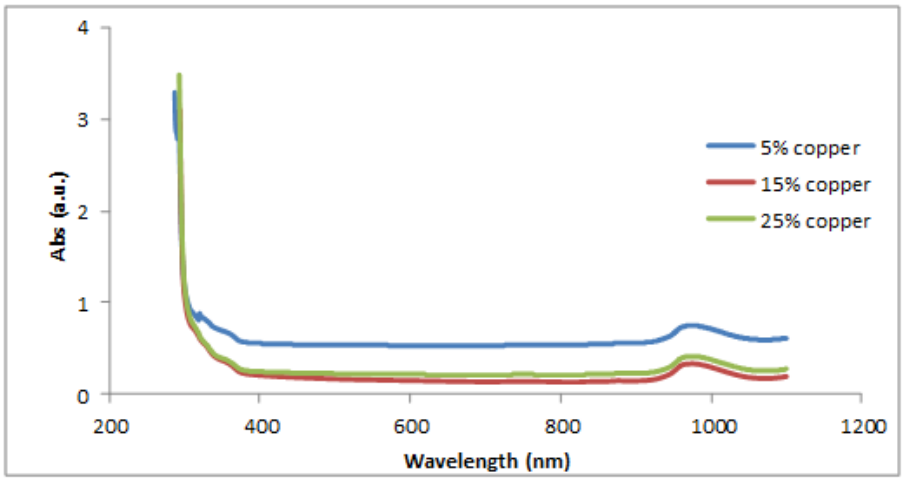

Fig. 12 - UV-Vis spectra of 5%, 15% and 25% copper composition annealed at 400°C

Table 2 below summarizes the optical band gap comparison of Fig. 7 to Fig. 9 according to composition and the annealing temperature. High temperature produced combination of amorphous crystalline constituents of the composites.

The shape of the grains (crystallites) is not uniform and it is said to be rutile. The grains of 5 wt% of copper are of stacked graphene (MWCNTs) and amorphous carbon at signature peaks at 26.5° and 44° respectively, and they are larger than that of 25 wt% due to the alignment created in the plane by increased copper concentration and temperature. Increase in the annealing temperature was noted to exfoliate the aggregates size in all the composition. The decrease in the grains size is observed to be proportional to the rise in temperature for both 5 and 25 wt% of copper analyzed with X-ray diffractometer. The band gap is observed to decrease with increasing copper wt% for as-grown. Much presence of graphite in the 5 wt% sample contributed to narrow band gap as the temperature increases because of the narrow optical band gap.

For both 15 and 25 wt% compositions, the band gap is noticed to increase with increasing temperature and this is attributed to the elastic/plastic alloy formed by copper and MWCNTs around 44°. Short duration annealing is observed to have a little lower band gap value to that of longer duration. This shows that, annealing duration contributes to optical property of a material. The thermal treatment of graphene oxide (GO) has been observed to cause changes in its quality, size and shape. Thermal treatment is known to cause pressure within the carbon planes of GO, as well as decomposition and expansion of GO layers to give CO_2, CO and H_2O gas [26] and such is the case with decomposition observed due to temperature rise. The thermal exfoliation process brought about more amorphous contents by reducing crystallinity and producing more elastic/plastic alloy within the composite's planes. Thus, this led to rise in band gap value.

Table 2 - Optical band gap variation with composition and temperature

% Copper	As-grown (eV)	200°C (12 hours) (eV)	400°C (12 hours) (eV)	400°C (6 hours) (eV)
5	4.16	4.15	4.15	4.14
15	4.13	4.13	4.15	4.15
25	4.10	4.15	4.16	4.15

4. Conclusion

Synthesis of graphene-copper composite was successfully carried out using hydrothermal method, which is considered simpler and more convenient than solvothermal method that requires alcohol, due to boiling point difference. The composites have shown wider optical band gaps which are between semiconductors and insulators and would be suitable for gas sensing, charge storage, electrodes among others. Annealing temperature is observed to be directly proportional to optical band gap for copper greater than 5 wt% and the effect of increased temperature resulted in grain refinement as a result of pressure /stress caused in the planes.

References

[1] Novoselov, K.S., Geim, A.K., Morozov, S.V., Jiang, D., Zhang, D., Dubonos, S.V., Grigorieva, I.V., & Firsov, A.A., (2004). Electric field effect in atomically thin carbon films. *Science 306*:666–669.

[2] Sekhar, C.R. (2015). Application of graphene and graphene-oxide based nanomaterials. Micro and nano technologies series, *Elsevier*, pp 1.

[3] Chae, H.K., Siberio-Perez, D.Y., Kim, J., Go, Y., Eddaoudi, M., Matzger, A.J., O'Keeffe, M., & Yaghi, O.M. (2004). A route to high surface area, porosity and inclusion of large molecules in crystals. *Nature, 427*, 523–527.

[4] Roberts, M.W., Clemons, C.B., Wilber, J.P., Young, G.W., Buldum, A., & Quinn, D.D. (2010). Continuum plate theory and atomistic modeling to find the flexural rigidity of a graphene sheet interacting with a substrate. *Journal of Nanotechnology, 2010*: 1-8.

[5] Muszynski, R., Seger, B., & Kamat, P.V. (2008). Decorating graphene sheets with gold nanoparticles. *The Journal of Physical Chemistry C, 112*(14), 5263-5266.

[6] Goncalves, G., Marques, P.A., Granadeiro, C.M., Nogueira, H.I., Singh, M.K., & Gracio, J. (2009). Surface modification of graphene nanosheets with gold nanoparticles: the role of oxygen moieties at graphene surface on gold nucleation and growth. *Chemistry of Materials, 21*(20), 4796-4802.

[7] Meyer, J.C., Geim, A.K., Katsnelson, M.I., Novoselov, K.S., Booth, T.J., & Roth, S. (2007). The structure of suspended graphene sheets. *Nature*, *446*(7131), 60-63.

[8] Santra, P.K., & Kamat, P.V. (2012). Mn-doped quantum dot sensitized solar cells: a strategy to boost efficiency over 5%. *Journal of the American Chemical Society*, *134*(5), 2508-2511.

[9] Akhavan, O., Ghaderi, E., & Rahighi, R. (2012). Toward single-DNA electrochemical biosensing by graphene nanowalls. *ACS nano*, *6*(4), 2904-2916.

[10] Singh, M., Goyal, M., & Devlal, K. (2018). Size and shape effects on the band gap of semiconductor compound nanomaterials. *Journal of Taibah University for Science*, *12*(4), 470-475.

[11] Jiang, H., Lee, P.S., & Li, C. (2013). 3D carbon based nanostructures for advanced supercapacitors. *Energy & Environmental Science*, *6*(1), 41-53.
[12] Yang, S., Feng, X., Ivanovici, S., & Müllen, K. (2010). Fabrication of graphene-encapsulated oxide nanoparticles: towards high-performance anode materials for lithium storage. *Angewandte Chemie International Edition*, *49*(45), 8408-8411.
[13] He, Y.S., Bai, D.W., Yang, X., Chen, J., Liao, X.Z., & Ma, Z.F. (2010). A Co (OH) 2− graphene nanosheets composite as a high performance anode material for rechargeable lithium batteries. *Electrochemistry Communications*, *12*(4), 570-573.
[14] Lu, J., He, Y.S., Cheng, C., Wang, Y., Qiu, L., Li, D., & Zou, D. (2013). Self-supporting graphene hydrogel film as an experimental platform to evaluate the potential of graphene for bone regeneration. *Advanced Functional Materials*, *23*(28), 3494-3502.
[15] [Han, T.H., Lee, Y., Choi, M.R., Woo, S.H., Bae, S.H., Hong, B.H., Ahn, J.H., & Lee, T.W. (2012). Extremely efficient flexible organic light-emitting diodes with modified graphene anode. *Nature Photonics*, *6*(2), 105-110.
[16] Rao, C.E.E., Sood, A.E., Subrahmanyam, K.E., & Govindaraj, A. (2009). Graphene: the new two-dimensional nanomaterial. *Angewandte Chemie International Edition*, *48*(42), 7752-7777.
[17] Tremel, A., Wasserscheid, P., Baldauf, M., & Hammer, T. (2015). Techno-economic analysis for the synthesis of liquid and gaseous fuels based on hydrogen production via electrolysis. *International Journal of Hydrogen Energy*, *40*(35), 11457-11464.
[18] Basu, S., & Hazra, S.K. (2017). Graphene–noble metal nano-composites and applications for hydrogen sensors. *C*, *3*(4), 29.
[19] Khan, M., Tahir, M.N., Adil, S.F., Khan, H.U., Siddiqui, M.R.H., Al-warthan, A.A., & Tremel, W. (2015). Graphene based metal and metal oxide nanocomposites: synthesis, properties and their applications. *Journal of Materials Chemistry A*, *3*(37), 18753-18808.
[20] Ni'maturrohmah, D., Maharani, D., Ruzicka, O., Gitasari, U.H., Adhitama, E., & Saraswati, T.E. (2018, March). Copper-graphene composite: electrochemical synthesis and structural characterization. *IOP Conference Series: Materials Science and Engineering*. *March*, *2018.* 333(1,) p. 012002.
[21] Zhang, J., Chen, Z., Zhao, J., & Jiang, Z. (2018). Microstructure and mechanical properties of aluminium-graphene composite powders produced by mechanical milling. *Mechanics of Advanced Materials and Modern Processes*, *4*(1), 1-9.
[22] Güler, Ö. (2014). Mechanical and thermal properties of a Cu-CNT composite with carbon nanotubes synthesized by CVD process. *Materials Testing*, *56*(9), 662-666.
[23] Moazzen, M., Khaneghah, A.M., Shariatifar, N., Ahmadloo, M., Eş, I., Baghani, A.N., Yousefinejad, S., Alimohammadi, M., Azari, A., Dobaradaran, S., Rastkari, N., Nazmara, S., Delikhoon, M., & Khaniki, G.J. (2019). Multi-walled carbon nanotubes modified with iron oxide and silver nanoparticles (MWCNT-Fe3O4/Ag) as a novel adsorbent for determining PAEs in carbonated soft drinks using magnetic SPE-GC/MS method. *Arabian Journal of Chemistry*, *12*(4), 476-488.
[24] [24Mohan, A.N., & Panicker, S. (2019). Facile synthesis of graphene-tin oxide nanocomposite derived from agricultural waste for enhanced antibacterial activity against Pseudomonas aeruginosa. *Scientific Reports*, *9*(1), 1-12.
[25] Licht, B.K., Homeyer, F., Bösebeck, K., Binnewies, M., & Heitjans, P. (2015). Synthesis and Electrochemical Behavior of Nanostructured Copper Particles on Graphite for Application in Lithium Ion Batteries. *Zeitschrift für Physikalische Chemie*, *229*(9), 1415-1427.
[26] Schniepp, H.C., Li, J.L., McAllister, M.J., Sai, H., Herrera-Alonso, M., Adamson, D.H., Prud'd+homme, R.K., Car, R., Saville, D.A., & Aksay, I.A. (2006). Functionalized single graphene sheets derived from splitting graphite oxide. *The journal of physical chemistry B*, *110*(17), 8535-8539.